NASA TECHNICAL NOTE

NASA TN D-2612

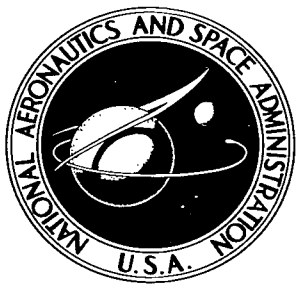

NASA TN D-2612

DIFFUSION OF AURORAL ELECTRONS IN THE ATMOSPHERE

by Kaichi Maeda

Goddard Space Flight Center
Greenbelt, Md.

NATIONAL AERONAUTICS AND SPACE ADMINISTRATION • WASHINGTON, D. C. • FEBRUARY 1965

DIFFUSION OF AURORAL ELECTRONS IN THE ATMOSPHERE

By Kaichi Maeda

Goddard Space Flight Center
Greenbelt, Md.

NATIONAL AERONAUTICS AND SPACE ADMINISTRATION

For sale by the Office of Technical Services, Department of Commerce,
Washington, D.C. 20230 -- Price $2.00

DIFFUSION OF AURORAL ELECTRONS IN THE ATMOSPHERE

by
Kaichi Maeda
Goddard Space Flight Center

SUMMARY

The results of a Monte Carlo computer program originally written by NBS to treat electron reflection and transmission by plane-parallel slabs are applied here to the diffusion of monoenergetic auroral electrons in the polar atmosphere. The following conclusions are reached: (1) The straggling effect is significant for electrons with energies above 20 kev, but is negligible below 10 kev. (2) Back-scattering decreases at both high and low energy levels, showing a maximum around 20 kev. The back-scattering coefficient at the maximum level is on the order of 7% (intensity) and 4% (energy flux) for vertical incidence, and 20% and 15% respectively, for isotropic incidence. (3) Angular distribution of penetrating electrons approaches perfect diffusion with cosine-squared rather than Gaussian distribution around half of the penetration (back-diffusion) depth for both vertical and isotropic incident distribution. Also, previous calculations on penetration depth and effective depth of energy distribution are shown to have been greatly underestimated for electron energies above 20 kev, because of the straggling effect.

CONTENTS

DIFFUSION OF AURORAL ELECTRONS IN THE ATMOSPHERE

by
Kaichi Maeda
Goddard Space Flight Center

INTRODUCTION

In calculating the rates of reactions caused by auroral activities (such as the vertical distributions of luminosity and auroral absorption or the rate of dissociation of air due to bombarding of auroral particles), it is necessary to have fundamental information on the behavior of electrons and other auroral particles in the upper atmosphere. One important aspect is the change of intensity (particle flux) and of energy flux, and the rate of change with atmospheric depth.

Intensities and energies of charged particles entering the atmosphere decrease with atmospheric depth. These changes and the associated rates of change are fairly accurately calculated by use of the so-called range-energy relations for most charged particles; but this is not the case for electrons (References 1-5). Because of the dominating effect of Coulomb scattering and its statistical nature in collision processes, changes of intensity and of energy of the electron flux penetrating the atmosphere were not rigorously calculated before the results of Spencer's extensive computations on energy dissipation of electrons in air became available (References 6 and 7).

Recently, M. H. Rees (Reference 8) made semi-empirical calculations of the luminosity distribution of aurorae, using laboratory data given by A. E. Grün (Reference 10). Since Grün's experiments were limited to the case of vertical incidence of monoenergetic electrons with energies from 5 to 54 kev, Rees had to make some *ad hoc* assumptions about the angular distribution in order to apply Grun's results to more general cases.

Another factor which makes theoretical calculations of electron-diffusion difficult is the so-called "straggling" effect. The importance of this effect has been shown by much laboratory data (References 9 to 11), but no calculations have been available for electrons diffusing in air with straggling as well as scattering and energy loss considered simultaneously.

At present, the only way of calculating electron diffusion including multiple Coulomb scattering and energy loss with its fluctuation is the Monte Carlo method. Many practical problems on irradiation by electrons have been solved by this method (References 12-14). A review of the method has been written by Berger (Reference 15), and details of these calculations are reported by Berger and Seltzer (References 16 and 17).

The main purpose of the calculations in this paper was originally to extend Spencer's work on the energy dissipation of electrons in air to energies below 25 kev, because most auroral electrons are in this energy range. Since the effect of straggling on the penetrating depth of electron flux (which is impossible to consider by Spencer's moments method) is rather important at higher energy, computations in this paper are extended above 25 kev.

It should be noted that the "tail," or low energy portion of the intensity curve of penetrating monoenergetic electrons, as shown by laboratory experiments, is due not only to the fluctuation in energy loss but also to scattering along the paths of penetrating electrons. Therefore, the word "straggling" is used in most cases for the effects due to both scattering and fluctuations in energy loss at each collision. In this paper, however, straggling means only the fluctuations in energy loss, the Landau fluctuation (Reference 18).

Since the geomagnetic field is nearly vertical and uniform in the polar region, unwinding of the spiral path of impinging electrons is equivalent to the oblique path with an indicent angle equal to the pitch angle (References 3 and 8). The results of the present calculations (which are performed with respect to air of uniform density without magnetic field) are, therefore, applied to electron diffusion in the polar upper atmosphere. Some examples of these applications are shown in the last section by making use of the CIRA (1961) model atmosphere.

CALCULATIONS

The Monte Carlo calculation consists essentially of two parts: the basic data which contain formulas for scattering and energy loss as a function of electron energy in the medium (i.e., in air); and the random sampling for combinations of these basic data for a given number of histories.

The programs for machine calculation have been made at several places for different purposes (References 12, 14, 15, 16, 17). Some of the details of the program (FORTRAN for IBM 7090) used in the present calculation are given by Berger (Reference 15).

The formulas used in the basic data are as follows:

Energy Loss

The energy range in the present calculation is between 2.5 kev and 200 kev. Therefore, the energy losses other than ionization loss can be neglected. Electron trajectories are schematically divided into a number of short sections, from which lengths are chosen so that the mean energy loss in each slab corresponds to a certain fraction of the incident energy $2^{-1/16}$ in most cases. The mean energy loss is calculated according to the Bethe theory which is formulated by Rohrlich and Carlson (Reference 19) as shown in Appendix A.

Scattering

The angular deflections of each electron trajectory with respect to the initial incident direction at the end of each slab, the thickness of which is specified as above, are calculated by the multiple scattering theory of Goudsmit and Saunderson (Reference 20) with Mott's cross-section for single scattering (Reference 21). A choice of the Goudsmit-Saunderson expression gives better accuracy for large deflection than the familiar Molière's formula (References 22 and 23).

Since the details of the calculations on scattering above are very lengthy and already written in a review article (Reference 15), only basic formulas are shown in Appendix B.

Straggling

The energy loss of an electron after traveling a certain path length is not unique but fluctuates around a certain mean value. The distribution of this fluctuation was first derived by Landau (Reference 18) under conditions in which the energy loss is very small as compared with the incident energy. Later this was refined by Blunck and Leisegang (Reference 24) taking into account effects of resonances due to the binding energies of orbital electrons. The result gives a wider broadening distribution than Landau's original distribution. In the calculations in this paper, an expression derived by Blunck and Leisegang as a convolution of the Landau distribution function and a Gaussian function is used. The final expression is shown in Appendix C. The former corresponds to broadening due to collisions with free electrons, i.e., bounding energies are neglected; while the latter corresponds to resonance-broadening due to collisions with bounded electrons.

The basic quantity to be computed is called the differential transmission T (Reference 15),

$$T = T(E_0, \cos\theta_0, E, \cos\theta, x)\, dE\, d(\cos\theta) \quad . \tag{1}$$

This quantity represents the probability that an electron, incident with energy E_0, at angle θ_0 from the normal direction, will emerge with energy E and at an angle θ (between $\cos\theta$ and $\cos\theta + d\cos\theta$) after traveling a slab of thickness x. Except for computations on back-scattering, all results are given for both vertical and isotropic incidence. Since the following expressions are the same for both cases, the initial angle θ_0 will be dropped in the expression of transmission T.

The thickness (or depth) x is expressed by the units of total range r_0 corresponding to initial energy E_0; that is, $x = r/r_0$ where r_0 and r are in units of gm/cm^2. The range r_0 is given by integrating

$$r_0 = \int_0^{E_0} \frac{dE}{-\frac{dE}{dr}} \tag{2}$$

with the Bethe formula for dE/dr as shown in Appendix B. E_0, r_0 and the altitude z_0, which corresponds to vertical depth r_0 in the CIRA (1961) model atmosphere are shown in Table 1.

Other Observable Quantities

Other observable quantities are calculated by integrating the differential transmission with respect to energy, to angle, or to both, as follows:

The relative differential energy spectrum at x, is given by

$$i(E_0, E', x)\, dE' = dE' \int_0^1 T(E_0, E', \cos\theta, x)\, d(\cos\theta) \quad . \quad (3)$$

The relative total intensity $I(E_0, x)/I_0$ is

$$\frac{I(E_0, x)}{I_0} = \int_{E_c}^{E_0} i(E_0, E', x)\, dE' \quad . \quad (4)$$

The relative energy flux is

$$\frac{E(x)}{E_0} = \frac{1}{E_0} \int_0^1 d(\cos\theta) \int_{E_c}^{E_0} E' \cdot T(E_0, E', \cos\theta, x)\, dE' \quad . \quad (5)$$

The angular distribution of relative intensity is

$$j(E_0, \cos\theta, x)\, d(\cos\theta) = d(\cos\theta) \int_{E_c}^{E_0} T(E_0, E', \cos\theta, x)\, dE' \quad . \quad (6)$$

The lower cut-off energy E_c is taken as 1 kev in all cases in the calculations in this paper. For the case of isotropic incidence, the calculations are done by integrating the initial distribution with respect to $\cos\theta_0$ with the weight function $\cos\theta_0$. Relative intensities are normalized to the initial intensity $I_0 = 10^4$.

Table 1

Initial Energy Correlated Against Range and Atmospheric Depth

E_0 (kev)	r_0 gm/cm^2	Z_0 (km)
2.5	2.76×10^{-5}	118.02
5.	8.79×10^{-5}	107.13
10.	2.909×10^{-4}	100.18
20.	9.824×10^{-4}	93.24
25.	1.455×10^{-3}	91.00
50.	4.924×10^{-3}	84.05
100.	1.627×10^{-2}	77.23
200.	5.0928×10^{-2}	70.73

RESULTS

Except for calculations of the angular dependence of back-scattering, the following results are based on the analyses of 2,000 Monte Carlo histories with two cases of incident distribution, the

one for vertical incidence and the other for isotropic incidence.* To see the effect of straggling, all calculations are done with and without straggling.

Relative Intensity $I(E_0, x)/I_0$

This is one of the most important points to be shown in the present calculations on electron diffusion in air and the results are shown in Figure 1 (a - f) for E_0 = 2.5, 5, 10, 20, 25, and 200 kev against depth x. Since these curves are almost identical for the cases with initial energies above 25 kev, those figures for 50 kev and 100 kev are omitted. Longer tails of intensity distributions, as given with straggling, are in better agreement with laboratory data than for those without straggling (References 9 and 10) although laboratory experiments are limited to the cases of vertical incidence.

Relative Energy Flux $E(x)/E_0$

The relative energy flux curves are shown in Figure 2 (a - f), corresponding to Figure 1 (a - f). Dashed lines shown in the case of E_0 = 25 kev and 200 kev (Figure 2(e) and (f)) indicate Spencer's result. Since Spencer's original results are given as the rate of energy dissipation (i.e., dE/dx), his result is shown after integrating his curves with respect to x. It should be noted that Spencer's calculations are done with respect to the unbounded homogeneous medium, while in the present computations, a computer program is written to treat the reflection and transmission of electrons by plane-parallel slabs, assuming that an electron, once it has left the slab, can never return to it.

Relative Energy Dissipation $dE/E_0\,dx$

By differentiating the energy-flux with respect to depth x, the relative energy dissipation curves are obtained as shown in Figure 3 (a - f) for E_0 = 2.5, 5, 10, 20, 25, and 200 kev. Since there is no large difference in these curves above E_0 = 25 kev, curves for E_0 = 50 and 100 kev are omitted. In this respect the conventional assumption of energy-independent relative dissipation curves, such as is made by Rees (Reference 8), is acceptable for electrons with energy above 25 kev up to around 500 kev, but is no longer accurate below 25 kev. A comparison with Spencer's result is shown in Figure 3(e) and (f) for the case of E_0 = 25 kev and 200 kev respectively with vertical incidence. The difference is significant both at the initial part and the tail part between the curve, with and without straggling.

Angular Dependence of Back-Scattering

The ratio of back-scattered to incident intensity (energy flux) is called the back-scattering coefficient or the back-diffusion coefficient (References 10 and 11).

*In order to check the accuracy of calculations on the energy dependence of the back-scattering coefficient, 10,000 histories are used for E_0 = 12.5 kev with two cases of vertical and isotropic incidence (Figure 5).

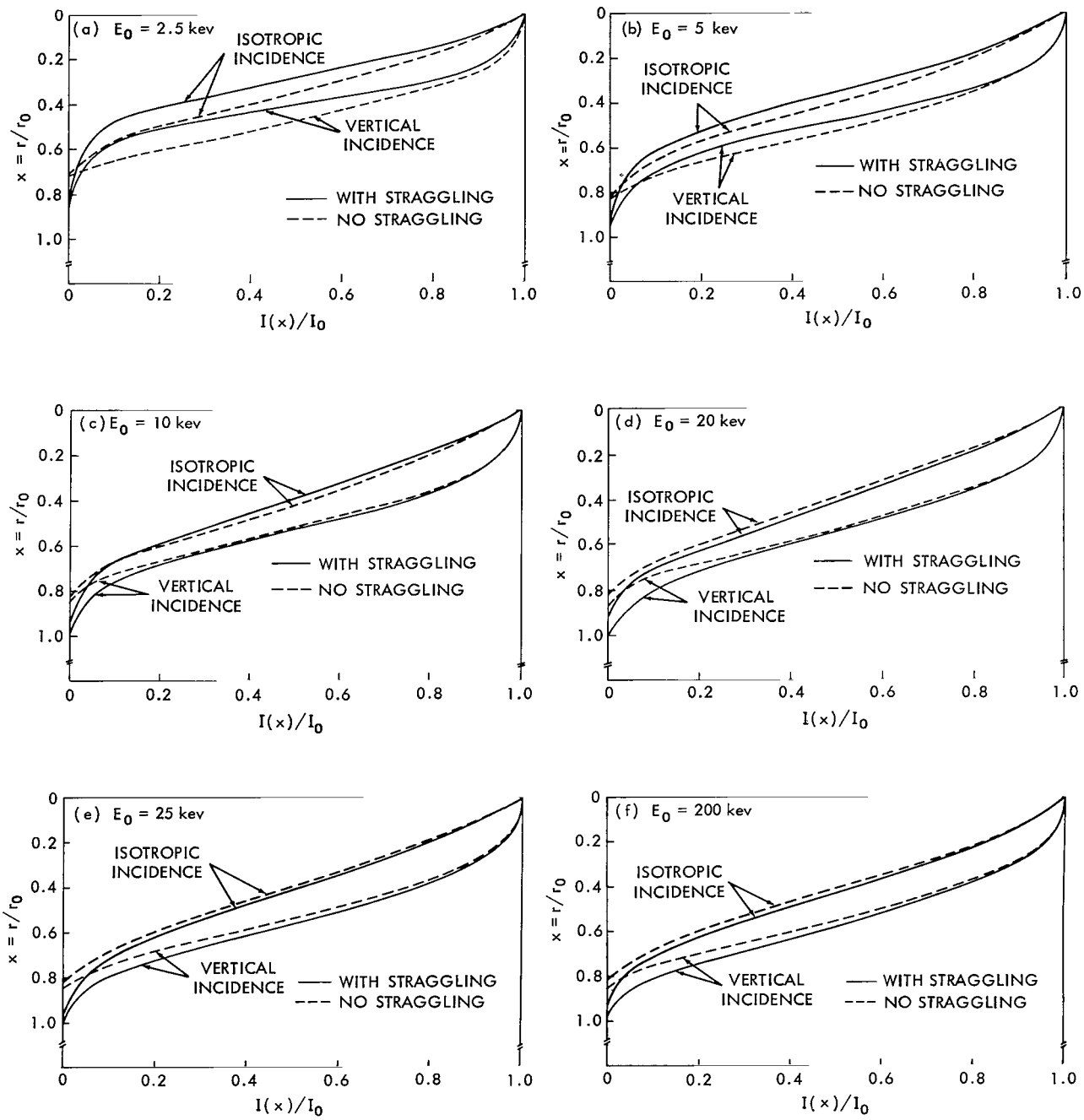

Figure 1—Relative intensities of penetrating monoenergetic electrons in air $I(x)/I_0$ vs. depth of air x, where $x = r/r_0$, and r_0 is the practical range of electrons, corresponding to the initial energy E_0 as shown in Table 1.

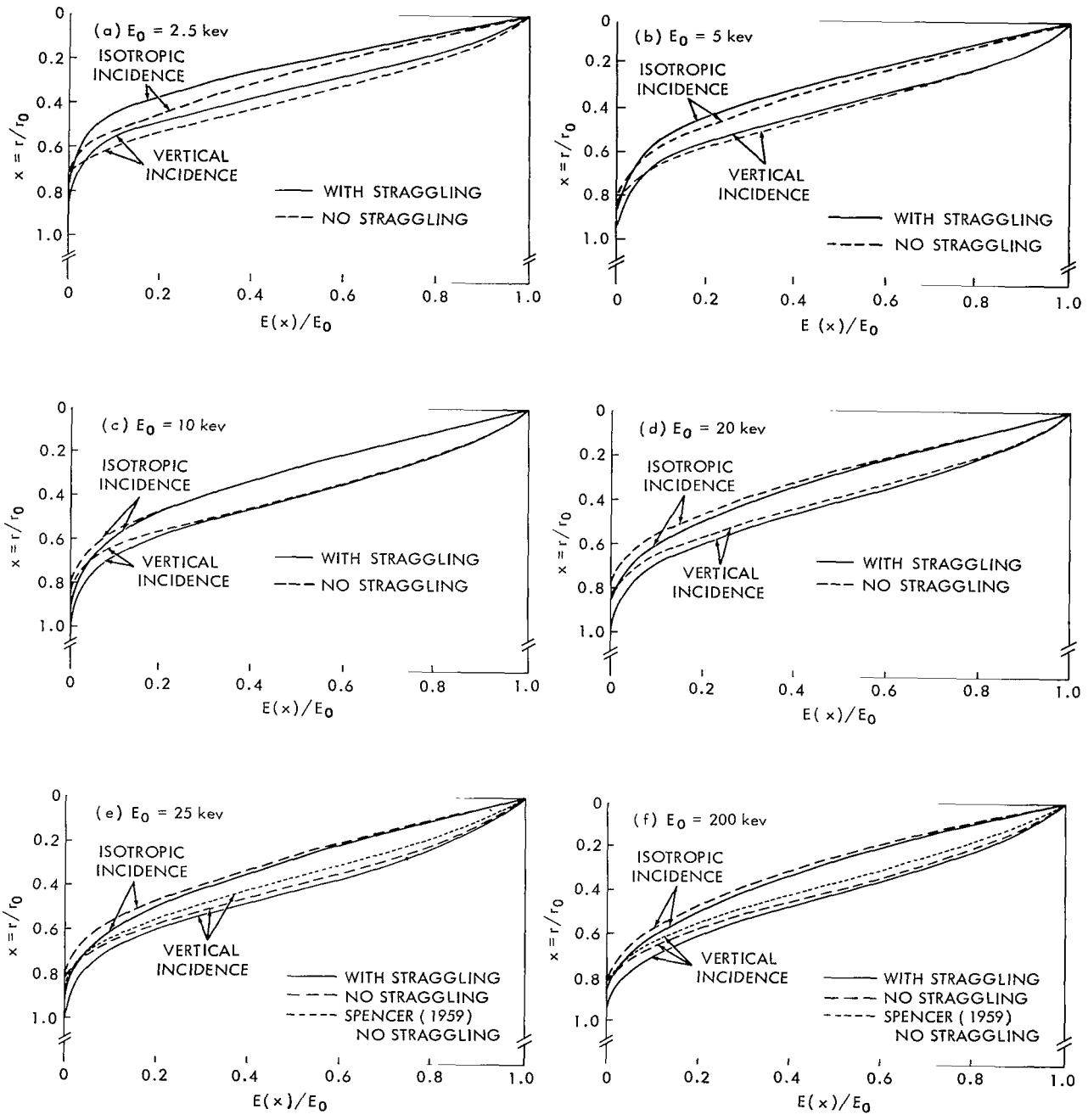

Figure 2—Relative energy flux of monoenergetic electrons $E(x)/E_0$ vs. the depth of air x, corresponding to the different initial energies shown in Figure 1.

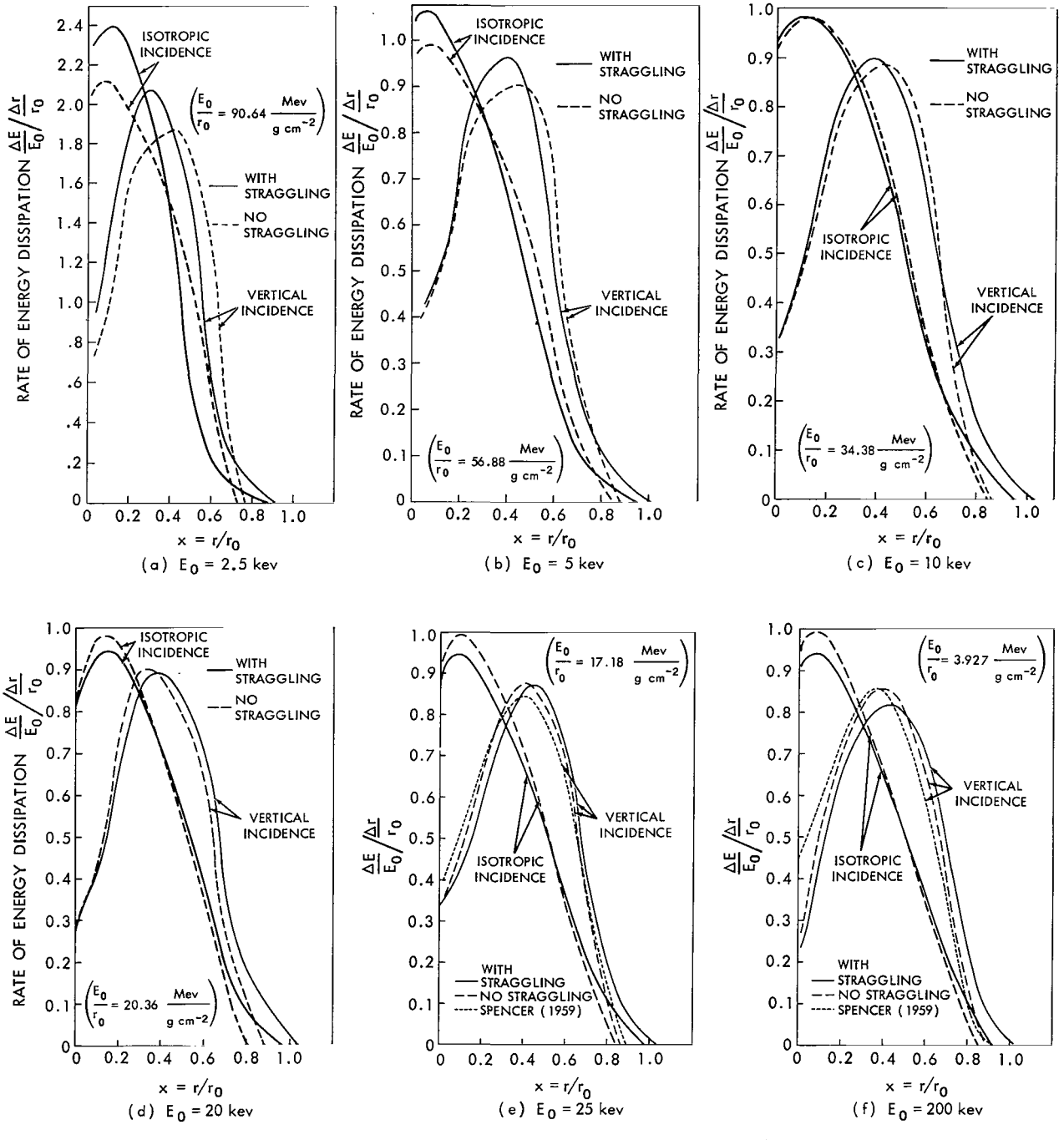

Figure 3—Relative energy dissipation curves of monoenergetic electrons $(\Delta E/E_0)/(\Delta r/r_0)$ vs. depth of air x, corresponding to the different initial energies shown in Figures 1 and 2.

Experimentally, it is known that this coefficient is quite large for materials with large atomic numbers, such as Pb ($Z = 82$) for which it is approximately 50%. On the other hand, this coefficient is regarded as negligible for materials like air that have small atomic numbers. Since laboratory measurements are limited to the case of vertical incidence, it is necessary to calculate them for the cases of oblique as well as isotropic incidence.

Figures 4 (a - f) show the angular dependence of this coefficient for incident energies of $E_0 = 2.5$, 5, 10, 20, 25, and 200 kev, both for intensity and for energy flux. Curves for $E_0 = 50$ and 100 kev are omitted, because there is no remarkable difference between curves above $E_0 = 25$ kev.

Energy Dependence of Back-Scattering

The results shown in Figure 4 are replotted against energies in Figures 5 (a and b) for vertical and isotropic incidence, respectively. A decrease of these coefficients with energy beyond 50 kev is experimentally well known (References 10, 11, and 13), although experiments are so far limited to normal incidence. It should be noted, however, that the coefficients also decrease below 10 kev, giving a maximum at around 20 kev for vertical incidence. On the other hand, in the case of isotropic incidence, a decrease of the back-scattering coefficient is very small and can be regarded as nearly constant between 20 kev and 500 kev. The values at the maximum are of the order of 7% for intensity (particle flux), and 4% for energy flux, in the case of vertical incidence. Corresponding values for isotropic incidence are 21% and 14% respectively. It is interesting to see that the effect of straggling is reversed around 10 kev for the case of isotropic incidence. This can be explained as follows: because of broadening in the energy distribution the number of low energy electrons increases, and their energies are so low that some of them are unable to leave the air even though they are back-scattered. On the other hand, decrease of back-scattering at high energies is simply due to the fact that the number density of scattered electrons concentrates in the forward direction in the laboratory system for high energy collisions, even though angular distributions of scattered electrons are isotropic in the center of a mass system of colliding electrons.

Applications for the Diffusion of Auroral Electrons

Figures 6 (a and b) show the intensity and energy flux distribution of monoenergetic 2.5 kev electrons in the atmosphere (CIRA, 1961) for vertical and isotropic incidence. Figures 7 (a, b) and Figures 8 (a, b) show similar curves for 20 kev and 200 kev electrons. From these figures, one can see that the effect of straggling is significant for electrons with energies higher than 20 kev: distribution of the greatest penetrating depth of vertically incident electrons exceeds the conventional penetration depth given by a range-energy relation based on a continuous ionization loss (Bethe formula). If the energy distribution is only due to multiple scattering, the greatest penetrating depth should never exceed the depth given by the Bethe formula. On the other hand, the effect of straggling is not important for electrons below 20 kev, and the effect is rather reversed below 10 kev; i.e., the greatest penetrating depth for straggling is less than the depth without straggling.

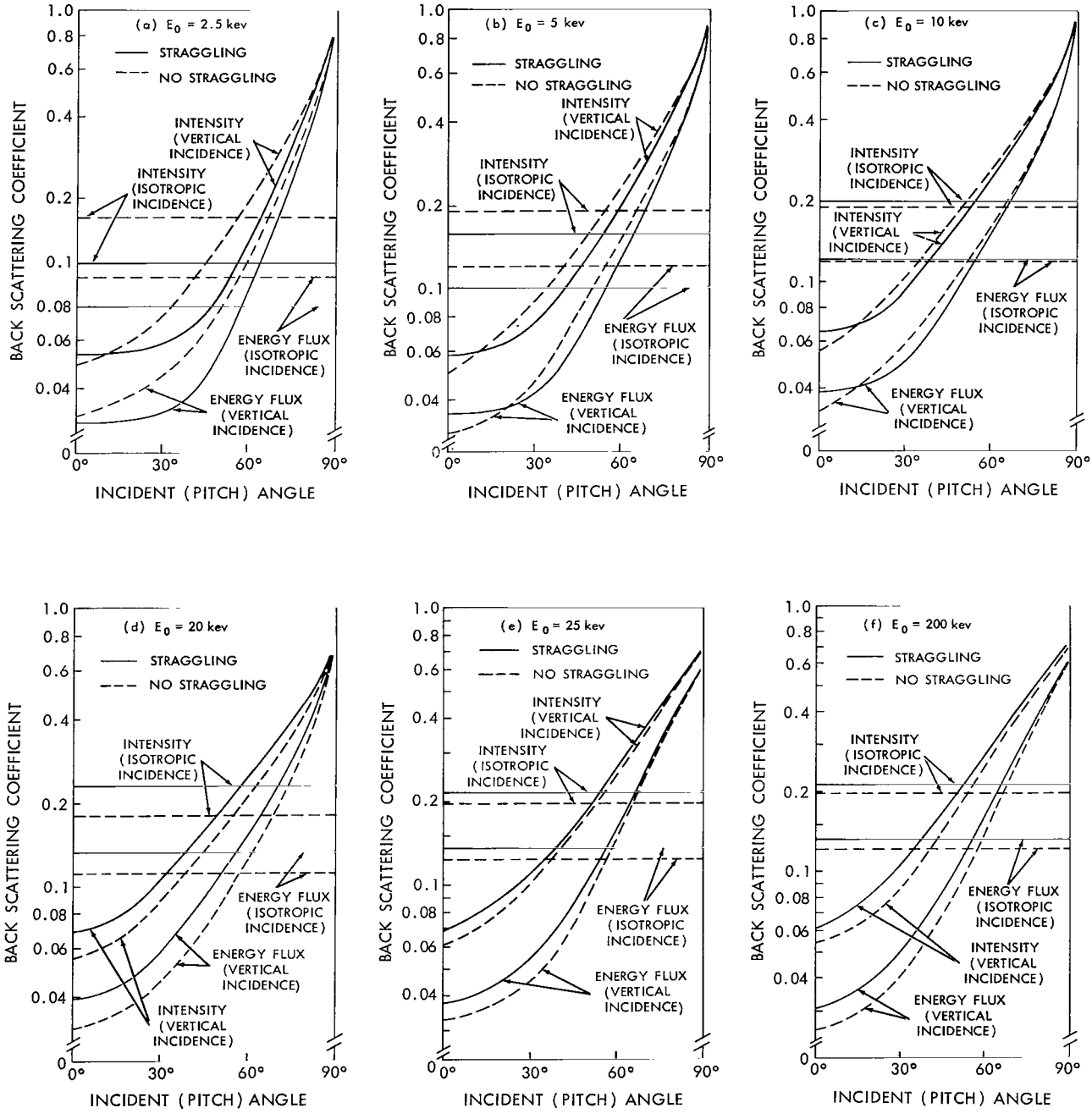

Figure 4—Back-scattering coefficient vs. incident (or pitch) angle of a monoenergetic electron beam.

By differentiating these energy flux functions with respect to altitude z, we can obtain the vertical distribution of energy dissipation of the primary electrons impinging into the atmosphere. One example, for 20 kev electrons is shown in Figure 9. Since $\Delta x = \bar{\rho} \cdot \Delta z$, where $\bar{\rho}$ is the mean air density between the level z and $z + \Delta z$, these curves can be also obtained directly from Figure 3, multiplying dE/dx curves by the value of atmospheric density at each level $\rho(x)$. We can see that the effect of straggling is not only to increase the penetration depth but also to shift the depth (i.e., height) of the maximum dissipation level. These curves can be compared with the vertical distribution of auroral luminosity (References 7 and 8).

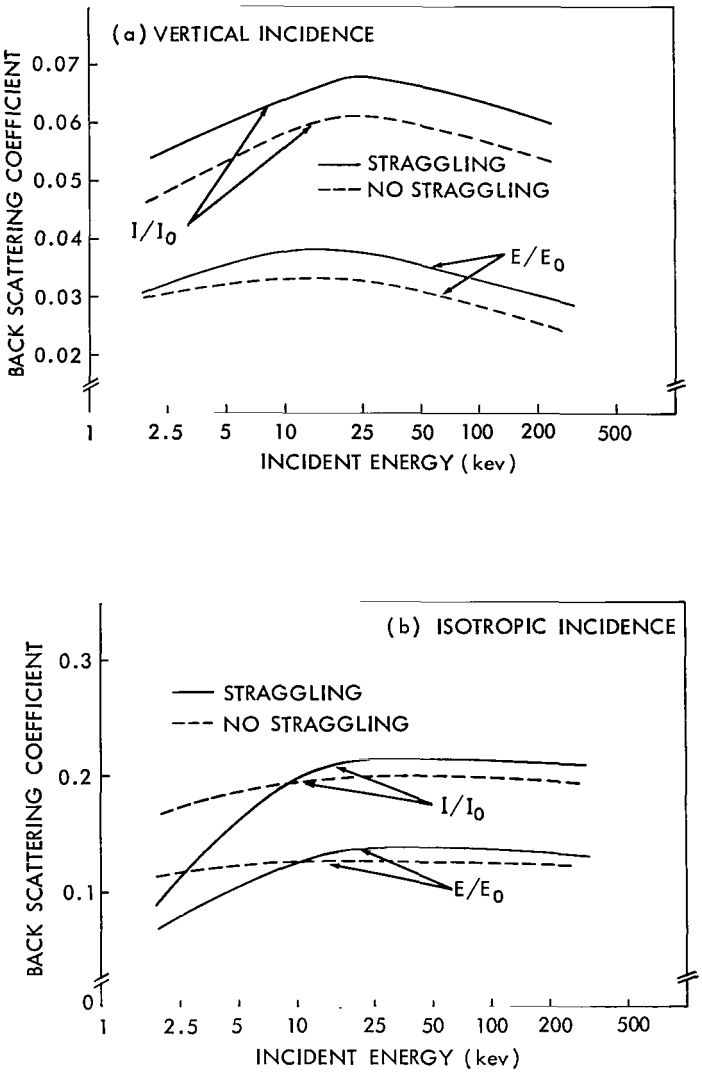

Figure 5—Back-scattering coefficients vs. incident energies for monoenergetic electrons at two angles of incidence.

Changes of angular distribution of monoenergetic 20 kev electrons, with altitude are shown in Figure 10 for vertical and isotropic incidence, with relative intensities normalized to initial intensity plotted against the cosines of the angle θ from the normal direction. Since the angular distribution for different energies is almost identical with respect to non-dimensional depth x; similar curves for other cases of different energies are omitted. It should be noted that the angular distribution rapidly approaches that of perfect diffusion with cosine-square distribution rather than Gaussian (Reference 11), around the half-depth of the maximum penetration for both vertical and isotropic incidence. Those depths are very close to the back-diffusion depth deducted from laboratory data on solid materials with vertical incidence (References 3 and 11). To show the transition into perfect diffusion with depth, a cosine-square curve is plotted by a dashed line in both figures for comparison. Another expression of these trends is shown in Figures 11 (a and b); where directional intensity is plotted against depth, x, for vertical and isotropic incidence. It should be noted that the number of electrons (intensity) diffusing into the oblique direction increases with depth until around one-third of the total penetration depth; intensities in the oblique direction show a maximum around one-third of the total

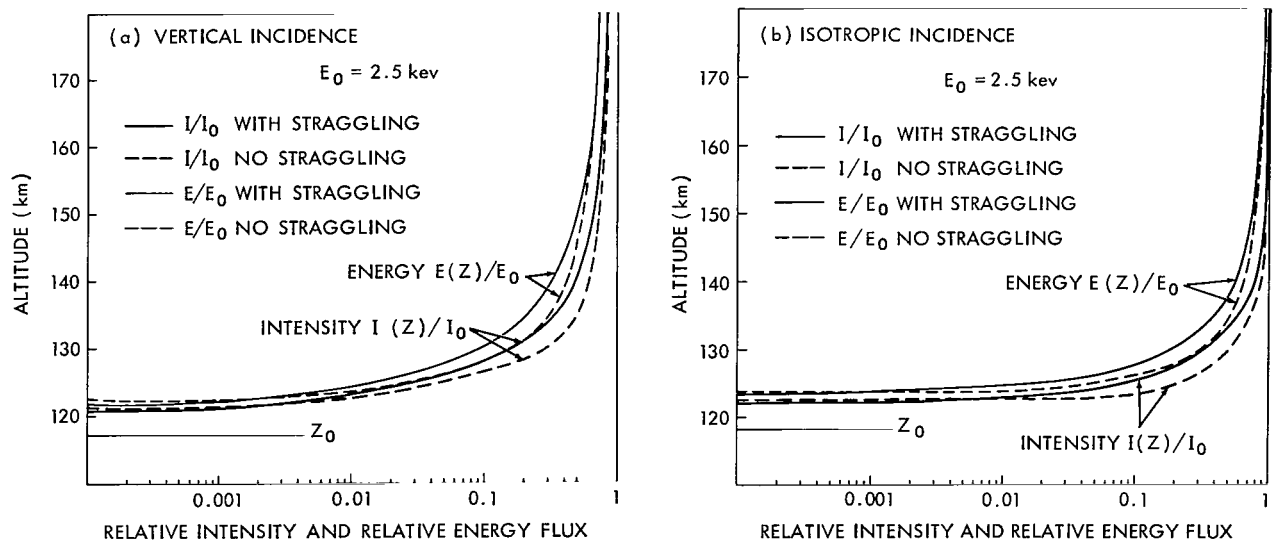

Figure 6—Relative intensity (particle flux) and relative energy flux (power) of electrons with an initial energy of 2.5 kev vs. altitude in the CIRA (1961) model atmosphere. The height Z_0 shows the maximum penetration depth (i.e., to the range r_0) for the initial electron energy E_0 as shown in Table 1.

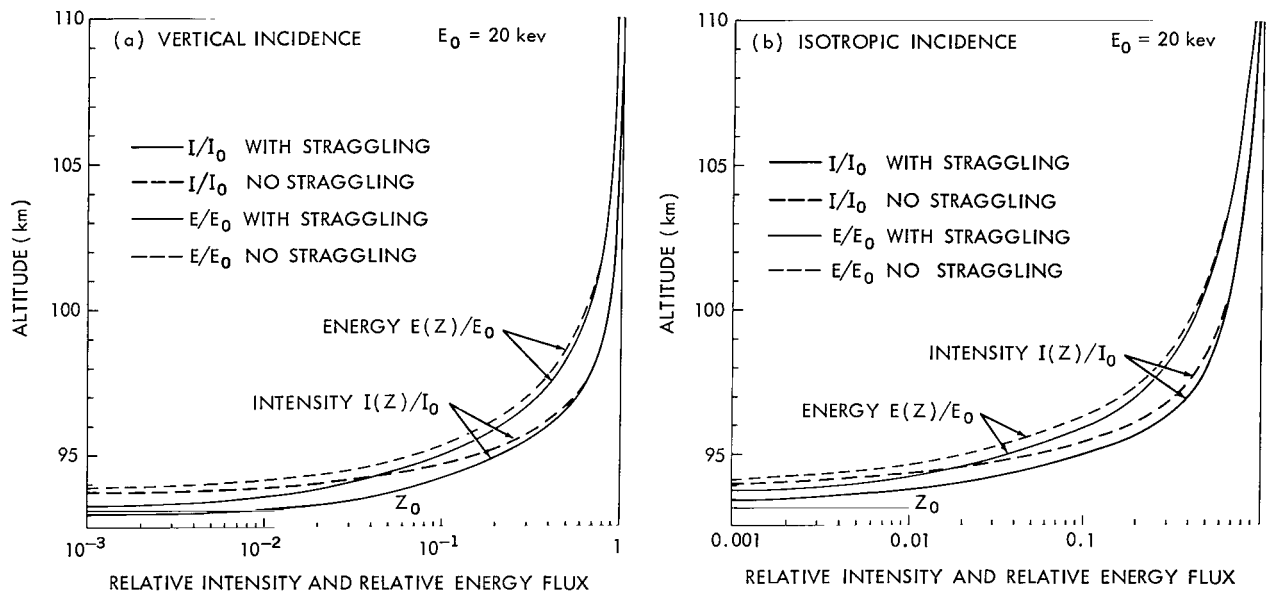

Figure 7—Relative intensity and relative energy flux of electrons with an initial energy E_0 = 20 kev vs. altitude in the CIRA (1961) model atmosphere.

penetration depth, while vertical intensity and all directional intensities with isotropic incidence decrease with penetrating depth monotonically. These curves are identical for different initial energies, as far as they have been plotted against non-dimensional depth $x = r/r_0$.

Finally, Figure 12 shows the differential energy spectrum of monoenergetic electrons (E_0 = 20 kev) incident in the atmosphere. Altitudes in parentheses are those in the CIRA (1961)

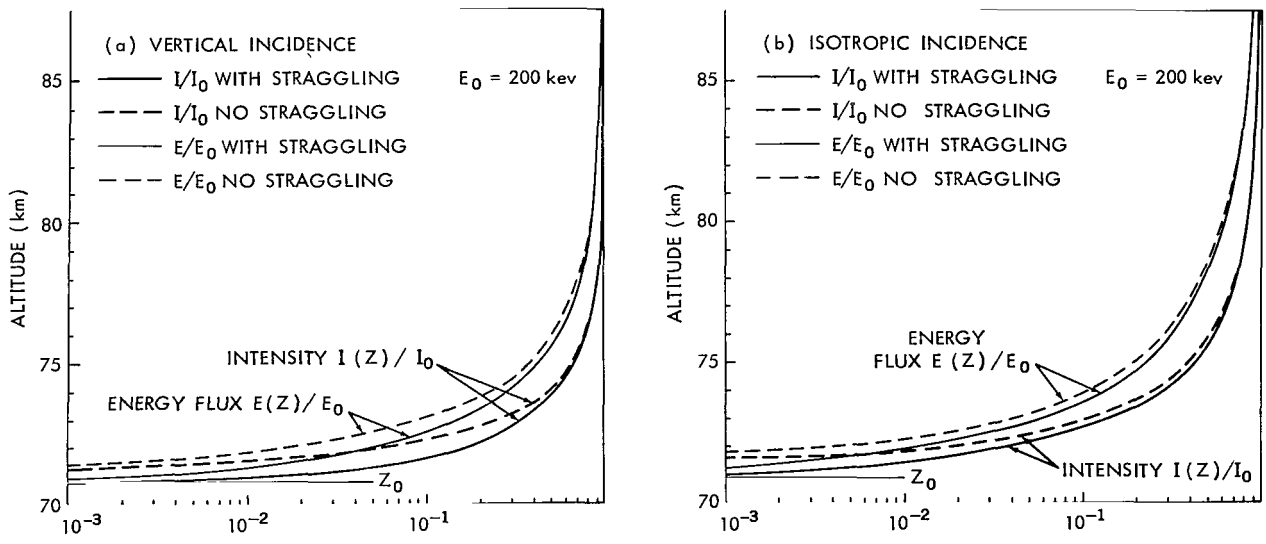

Figure 8—Relative intensity and relative energy flux of electrons with an initial energy E_0 = 200 kev vs. altitude in the CIRA (1961) model atmosphere.

atmosphere corresponding to the depth x, with $r_0 = 9.8237 \times 10^{-4}$ for 20 kev (Table 1). At the bottom, energies correspond to the continuous energy-range relation:

$$E_m = E_0 - \int_0^x \frac{dE}{dx'} dx' \qquad (7)$$

where dE/dx' is given by the Bethe theory (Appendix A), are shown. It should be noted that energies corresponding to maximum intensities for each depth are slightly lower than E_m. The relative change-of-energy spectrum is almost the same for different initial energies below 200 kev, provided that these are plotted with the non-dimensional parameter x.

CONCLUSIONS

Summarizing the present results, we can state the following points:

(1) Previous estimations of intensities (particle flux) and energy flux (powers)

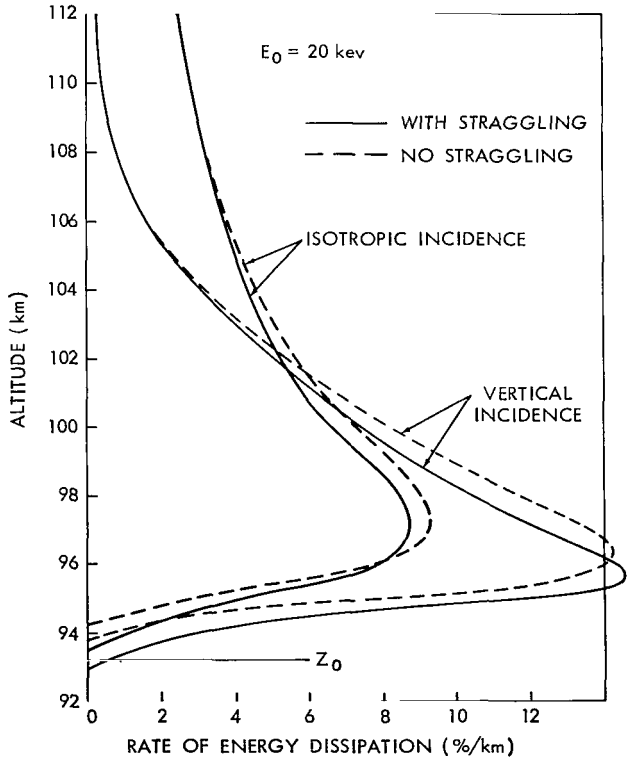

Figure 9—Energy dissipation curves for electrons with initial energy E_0 = 20 kev in the CIRA (1961) model atmosphere.

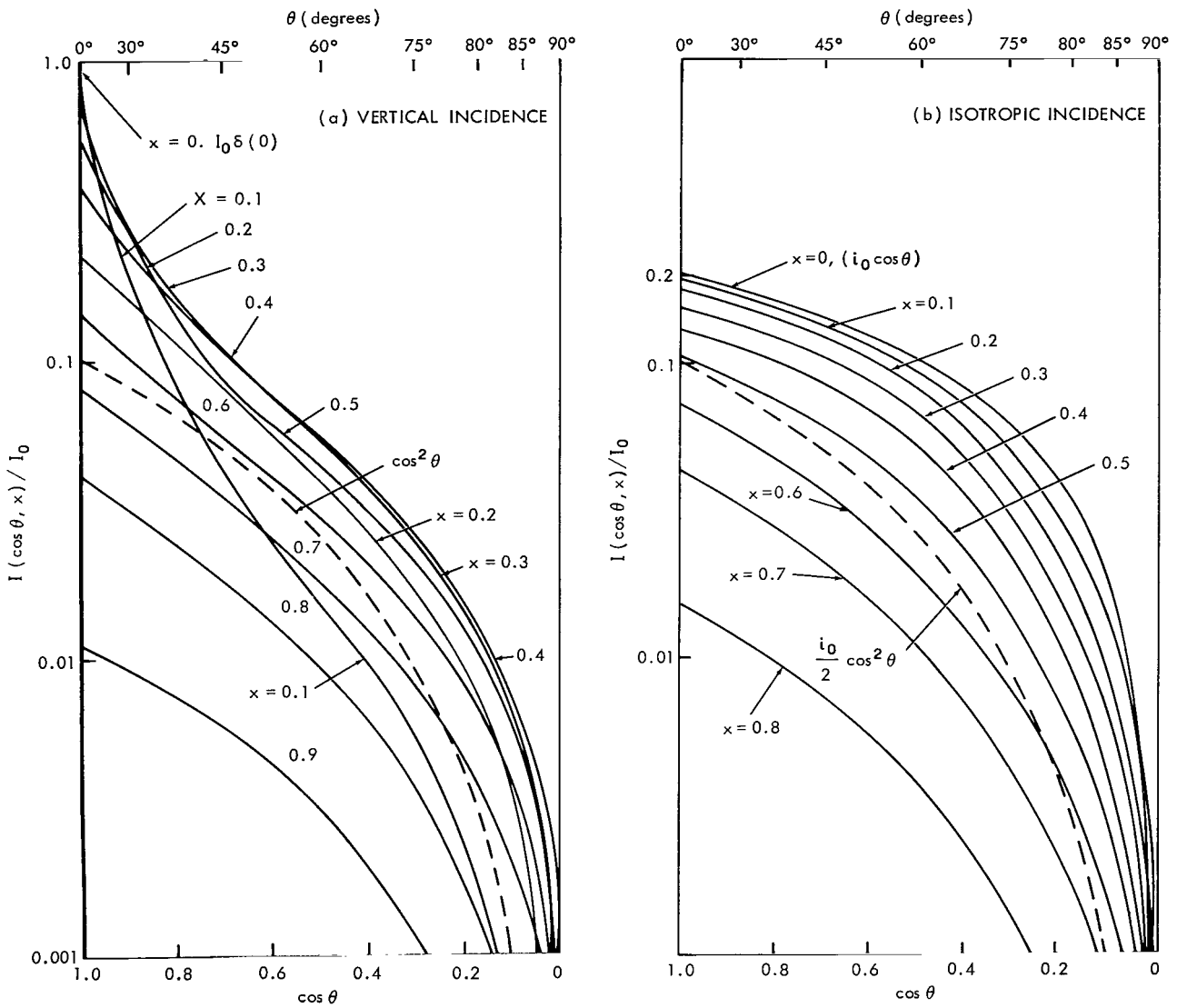

Figure 10—Angular distribution (relative intensity/steradian) of electrons with an initial energy E_0 at different atmospheric depths. Although based on the results of E_0 = 20 kev, these curves are nearly identical for all values of E_0 below 200 kev, since they are plotted with the non-dimensional parameter $x = r/r_0$ as used in Figures 1, 2, and 3. The heavy curve to the initial distribution, i.e., $\delta(0)$ for vertical incidence and 1/2 cos θ for isotropic incidence; and the dashed curves indicate the $\cos^2 \theta$ curve for comparison.

of penetrating electrons in air (based on the so-called range-energy relation) have been significantly underestimated, as can be seen from Figures 1, 2 and 12. For electrons with energies above 20 kev, the greatest penetration depth and the depth of maximum energy dissipation are deeper than those previously estimated by neglecting straggling (Figures 3 and 9).

(2) Straggling is negligible below 10 kev and the effect is rather opposite to that for energies above 20 kev (Figures 1a, 1b, 2a, 2b, 3a, and 3b).

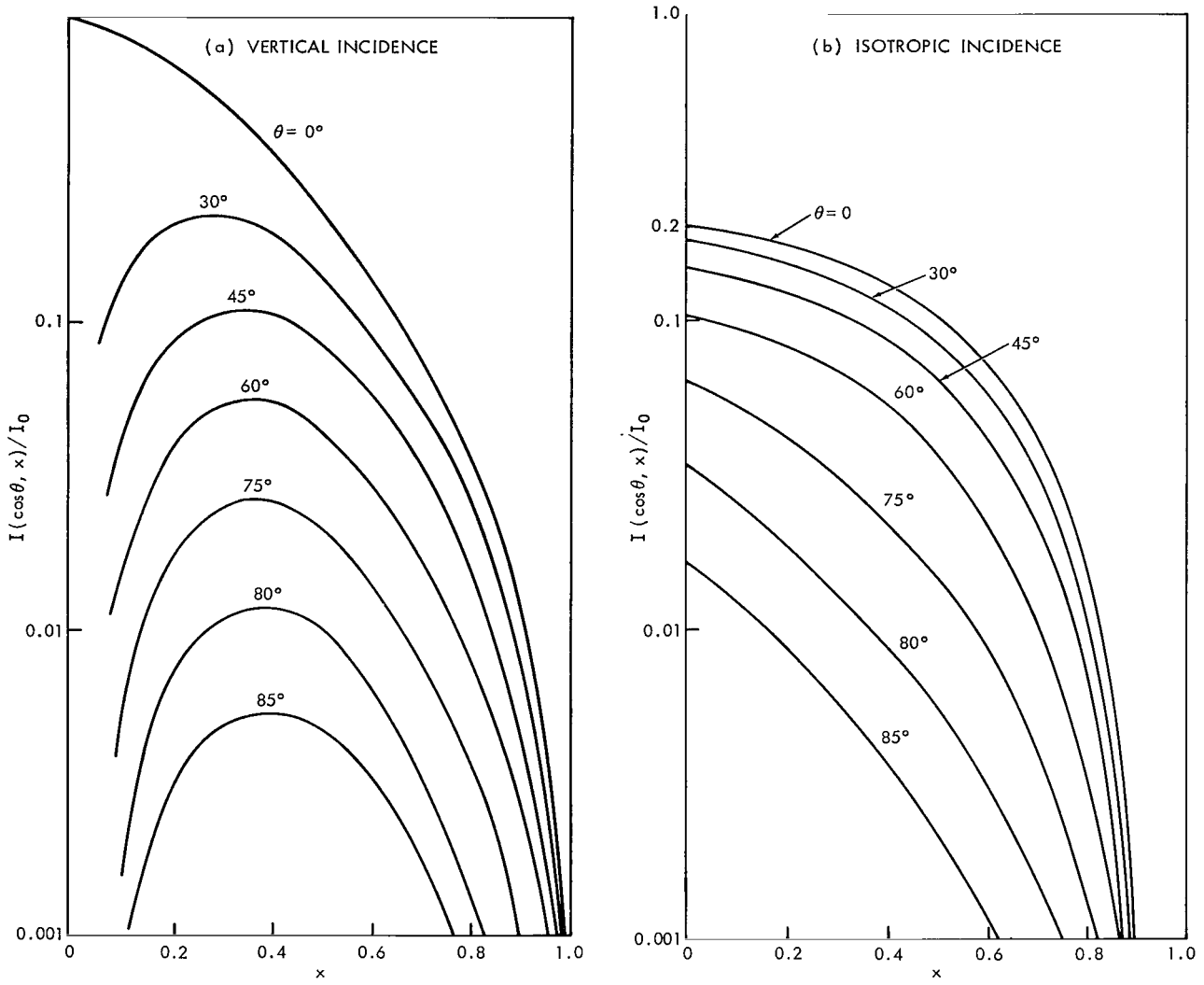

Figure 11—Plots of relative intensity (similar to Figure 10) against non-dimensional depth $x = r/r_0$ with the parameter θ, the angle from the vertical (incident) direction.

(3) The back-scattering coefficient decreases at both high and low energies, showing a maximum around 20 kev. The values of this coefficient at the maximum are approximately 7% for intensity (particle flux) and 4% for energy flux (power), in the case of vertical incidence. Corresponding values in the case of isotropic incidence are 21% and 14%, respectively (Figures 5a and 5b).

(4) Back-scattering is nearly constant above 20 kev up to 500 kev for electrons with isotropic incidence, although the back-scattering coefficient decreases slightly with energy, for both cases of incident angular distribution as can be seen from Figure 5.

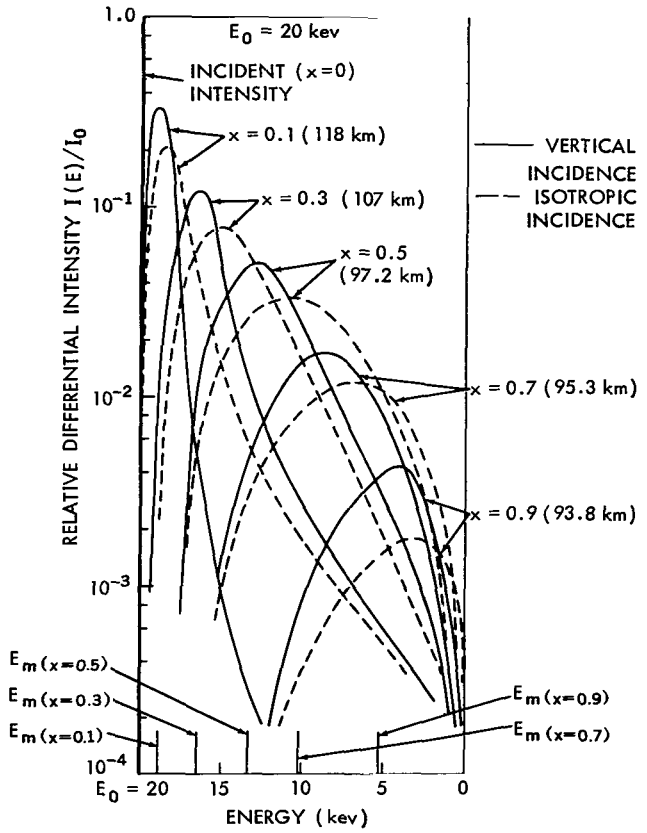

Figure 12—Differential energy spectrum of monoenergetic electrons, E_0 = 20 kev incident in the atmosphere.

(5) The angular distribution of penetrating electrons approaches that for perfect diffusion with cosine-square distribution rather than Gaussian, within less than half of the penetration depth for both vertical and isotropic incidence, as can be seen from Figures 10 and 11. This depth is very close to the so-called back-diffusion thickness deduced from laboratory data, based on vertical incidence and on solid materials (References 3 and 11).

(6) The energy spectrum of monoenergetic incident electrons spreads rapidly with penetrating depth, due to both multiple Coulomb scattering and straggling. The maximum intensities of these energy spectra at each depth are slightly lower than those corresponding to the ones given by the conventional range-energy relation, particularly near the end of the range and for the electrons with isotropic incidence (Figure 12).

Finally, it should be noted that the present calculations are based on a computer program which was written to treat the reflection and transmission of electrons by plane-parallel slabs, where the possibility of multiple traversal of slab boundaries was assumed to be zero. In application to atmospheric diffusion, it would be more accurate to allow this possibility, treating the atmosphere as a semi-infinite medium. Although it is not expected that this will change the results of the present calculations very much, as was mentioned in the discussion of the relative energy flux, new studies are in progress to include this possibility. It is more important, however, to take into account the effect of the earth's magnetic field. This will also be done in the near future, and the effect of the uniform magnetic field on the paths of scattered electrons in air will be considered.

ACKNOWLEDGMENT

The author is very grateful to Dr. M. J. Berger and Mr. S. M. Seltzer in the National Bureau of Standards, who have developed most of the FORTRAN Programs used in the present calculations.

Manuscript received June 12, 1964.

REFERENCES

1. Rossi, B., "High Energy Particles," New York: Prentice-Hall, Inc., 1952, p. 438.

2. Maeda, K., and Singer, S. F., "Energy Dissipation of Spiraling Particles in the Polar Atmosphere," *Arkiv Geofyzik* 32, paper 21, 531-538, 1961.

3. Maeda, K., "Auroral Dissociation of Molecular Oxygen in the Polar Mesosphere," *J. Geophys. Res.* 68(1):185-197, January 1, 1963.

4. Maeda, K., "On the Heating of the Polar Night Mesosphere, Part I," *Meteorol. Abhandl. Freie Universität Berlin Inst. für Meteorol. und Geophys.* 36:451-496, 1963.

5. Maeda, K., "On the Zenithal Distribution of Extremely-High-Energy Cosmic Ray Muons in the Atmosphere," *J. Geophys. Res.* 69(9):1725-1736, May 1, 1964.

6. Spencer, L. V., "Energy Dissipation by Fast Electrons," National Bureau of Standards Monograph 1, Washington: U.S. Department of Commerce, National Bureau of Standards, 1959.

7. Chamberlain, Joseph W., "Physics of the Aurora and Airglow," New York: Academic Press, 1961, p. 286.

8. Rees, M. H., "Auroral Ionization and Excitation by Incident Energetic Electrons," *Planetary Space Sci.* 11:1209-1218, October 1963.

9. Grün, A. E., "Lumineszenz - Photometrische Messungen der Energieabsorption im Strahlungsfeld von Elektronenquellen. Eindimensionaler Fall in Luft," *Z. Naturforsch.* 12A(2), 89-95, 1957.

10. Frank, H., "Zur Vielfachstreung und Rück-diffusion schneller Elektronen nach Durchgang durch dicke Schichten," *Z. Naturforsch.* 14A(3), 247-261, March 1959.

11. Wu, C. S., "The Interaction of Beta Particles with Matter," in: *Nuclear Spectroscopy, Part A,* ed. by Fay Ajzenberg-Selove, New York: Academic Press, 1960, pp. 15-30.

12. Sidei, T., Higashimura, T., and Kinosita, K., "Monte Carlo Calculation of the Multiple Scattering of the Electron," *Mem. Fac. Engr., Kyoto University* 19(2), 220-228, April 1957.

13. Perkins, J. F., "Monte Carlo Calculation of Transport of Fast Electrons," *Phys. Rev.* 126(5), 1781-1784, June 1, 1962.

14. McGarrigle, K. S., and Mar, B. W., "Electron Monte Carlo," Report D2-90418-5, Boeing Co., 1963.

15. Berger, Martin J., "Monte Carlo Calculation of the Penetration and Diffusion of Fast Charged Particles," in: *Methods of Computational Physics, Vol. I,* New York: Academic Press, 1963.

16. Berger, M. J., and Seltzer, S. M., "Energy Spectra and Angular Distributions of Electrons Transmitted through Sapphire (Al_2O_3) Foils," Report SP-3008, Washington: National Aeronautics and Space Administration, 1964.

17. Berger, M J., and Seltzer, S. M., "Tables of Energy Losses and Range of Electrons and Positrons," NAS-NRC Publication No. 1133, Nuclear Science Series Report 39, Washington: National Academy of Sciences - National Research Council, 1964.

18. Landau, L., "On the Energy Loss of Fast Particles by Ionization," *J. Phys. (Acad. Sci. USSR)* 8(4), 201-205, 1944.

19. Rohrlich, F., and Carlson, B. C., "Positron - Electron Differences in Energy Loss and Multiple Scattering," *Phys. Rev.* 93, 38-44, January 1, 1954.

20. Goudsmit, S., and Saunderson, J. L., "Multiple Scattering of Electrons," *Phys. Rev.* 57, 24-29, January 1, 1940.

21. Mott, N. F., "The Scattering of Fast Electrons by Atomic Nuclei," *Proc. Roy. Soc.* A124, 425-442, June 4, 1929.

22. Bethe, H. A., "Molière's Theory of Multiple Scattering," *Phys. Rev.* 89, 1256-1266, March 15, 1953.

23. Bethe, H. A., and Ashkin, J., "Passage of Radiations Through Matter," in: *Experimental Nuclear Physics, Volume I,* ed. by E. Segre, New York: John Wiley, Inc., 1960, pp. 166-357.

24. Blunck, O., and Leisegang, S., "Zum Energieverlust Schneller Elektronen in Dünner Schichten," *Zeits. Phys.* 128(4), 500-505, 1950.

25. O'Brien, B. J., "Lifetime of Outer-Zone Electrons and their Precipitation into the Atmosphere," *J. Geophys. Res.* 67(10), 3687-3706, September 1962.

Appendix A

Energy Loss Along the Electron Path

Since radiation losses (including loss due to direct pair-production) are negligible below 200 kev, the following formula for ionization loss is used for continuous energy loss along the paths of electrons (References 15 and 19):

$$-\frac{1}{\rho}\left(\frac{dE}{dx}\right) = \frac{2\pi N_a r_0^2 mc^2}{\beta^2} \cdot \frac{Z}{A}\left[\ln \frac{\tau(\tau+2)}{2\left(\frac{I}{mc^2}\right)^2} + F(\tau) - \delta\right], \qquad \text{(A1)}$$

where

$$F(\tau) = \left[1 + \frac{\tau^2}{8} - (2\tau + 1)\ln 2\right] / (\tau + 1)^2$$

δ = Correction factor for the density effect (practically zero for air below 200 kev electrons),

τ = Kinetic energy in units of electron rest mass,

mc^2 = Rest mass of electron, 5.1098×10^5 ev,

γ = Classical radius of electron, 2.8178×10^{-13} cm, e^2/mc^2,

N_a = Avogadro's number, 6.02492×10^{23} mol^{-1},

β = Velocity of electron in units of light velocity, $c = 2.9979 \times 10^{10}$ cm/sec.

The quantities ρ, Z/A and I are defined by the following mean value formula;

$$\rho = \sum_i \rho_i ,$$

$$\frac{Z}{A} = \frac{1}{\rho}\sum_i \frac{Z_i}{A_i}\rho_i ,$$

and

$$I = \left(\frac{Z}{A}\right)^{-1} \cdot \frac{1}{\rho}\sum_i \frac{Z_i}{A_i}\rho_i ,$$

where ρ_i, Z_i, A_i and I_i are the density (gm/cm^3), atomic number, mass number and ionization potential (ev) of the three principal elements present in air and of air itself, as shown in Table A1. In the table, the relative abundance in mass ρ_i/ρ is also shown.

Table A1

Atomic numbers, mass numbers, ionization potentials, and relative abundances of atmospheric constituents.

Element	Atomic Number	Mass Number	Ionization Potential (ev)	ρ_i/ρ
O	8	16	89	0.232
N	7	14	85	0.755
A	18	40	210	0.013
air	7.37	14.3	87	1.000

Appendix B

Angular Deflection of a Scattered Electron

Angular deflection: Following from the work of Goudsmit and Saunderson (Reference 20), the angular multiple-scattering distribution $f(\omega)$, is given by

$$f(\omega) = \sum_{l=0}^{\infty} \left(l + \frac{1}{2}\right) \exp\left[-\int_0^s G_l(s')\,ds'\right] P_l(\cos\omega) , \tag{B1}$$

where ω is a deflection angle of a trajectory after passing a path length s from the initial incident direction, and $G(s')$ is given as a function of single Coulomb scattering cross-section $\sigma(\theta, s)$, i.e.,

$$G_l(s) = 2\pi N \int_0^{\pi} \sigma(\theta, s)\left[1 - P_l(\cos\theta)\right] d(\cos\theta) . \tag{B2}$$

Integration of $G_l(s)$ with respect to path length s has been done by making a transform on s for a given expression of $\sigma(\theta, s)$ (Reference 15), and a given number density for the medium (i.e., air). The simplest formula for $\sigma(\theta, s)$ is the Rutherford formula which is corrected for the screening effect due to orbital electrons by Mott (Reference 21). It should be noted that the dependence of $\sigma(\theta, s)$ on the path length s is derived from its well known energy dependence, $\sigma(\theta, E)$.

Appendix C

Distribution of Fluctuating Energy Loss

The distribution of the fluctuating energy loss ΔE of electrons, $W(\Delta E)$, with initial energy E_0 after traveling a path length s, around a mean value $\overline{\Delta E}$, which corresponds to a loss rate given in Appendix A, is given by Blunck and Leisegang as:

$$W(\Delta E)\, d(\Delta E) = \sum_{\nu} \frac{c_\nu \cdot \gamma_\nu}{\sqrt{\gamma_\nu^2 + b^2}} \exp\left[-\frac{(\lambda - \lambda_\nu)^2}{\gamma_\nu^2 + b^2}\right], \tag{C1}$$

where

$$b = \sqrt{\frac{5.6}{a \cdot s}},$$

$$a = 154 \frac{Z}{A} \cdot \frac{\rho}{\beta^2},$$

and

$$\lambda = \frac{\Delta E - \overline{\Delta E}}{a \cdot s} + \ln\left(\frac{E_0}{a \cdot s}\right) - 1.116 .$$

The constants c_ν, λ_ν and γ_ν are shown in Table C1.

It should be noted that the probability distribution function (C1) is derived by making use of a convolution of the Landau function with a Gaussian function. The latter corresponds to the resonance effect due to bounded electrons in the medium, which is neglected in Landau's theory (Reference 24).

Table C1

The constants c_ν, λ_ν, and γ_ν.

Constant	$\nu = 1$	$\nu = 2$	$\nu = 3$	$\nu = 4$
c_ν	0.174	0.058	0.019	0.007
λ_ν	0.0	3.0	6.5	11.0
γ_ν	1.8	2.0	3.0	5.0

NASA-Langley, 1965 G-589

"The aeronautical and space activities of the United States shall be conducted so as to contribute . . . to the expansion of human knowledge of phenomena in the atmosphere and space. The Administration shall provide for the widest practicable and appropriate dissemination of information concerning its activities and the results thereof."

—NATIONAL AERONAUTICS AND SPACE ACT OF 1958

NASA SCIENTIFIC AND TECHNICAL PUBLICATIONS

TECHNICAL REPORTS: Scientific and technical information considered important, complete, and a lasting contribution to existing knowledge.

TECHNICAL NOTES: Information less broad in scope but nevertheless of importance as a contribution to existing knowledge.

TECHNICAL MEMORANDUMS: Information receiving limited distribution because of preliminary data, security classification, or other reasons.

CONTRACTOR REPORTS: Technical information generated in connection with a NASA contract or grant and released under NASA auspices.

TECHNICAL TRANSLATIONS: Information published in a foreign language considered to merit NASA distribution in English.

TECHNICAL REPRINTS: Information derived from NASA activities and initially published in the form of journal articles.

SPECIAL PUBLICATIONS: Information derived from or of value to NASA activities but not necessarily reporting the results of individual NASA-programmed scientific efforts. Publications include conference proceedings, monographs, data compilations, handbooks, sourcebooks, and special bibliographies.

Details on the availability of these publications may be obtained from:

SCIENTIFIC AND TECHNICAL INFORMATION DIVISION

NATIONAL AERONAUTICS AND SPACE ADMINISTRATION

Washington, D.C. 20546